Journal of Pharmaceutical Analysis 2014;4(2):81–95

Contents lists available at ScienceDirect

Journal of Pharmaceutical Analysis

www.elsevier.com/locate/jpa
www.sciencedirect.com

ORIGINAL ARTICLE

Charge-transfer interaction of drug quinidine with quinol, picric acid and DDQ: Spectroscopic characterization and biological activity studies towards understanding the drug–receptor mechanism

Hala H. Eldaroti[a,*], Suad A. Gadir[a], Moamen S. Refat[b,c], Abdel Majid A. Adam[b]

[a]*Department of Chemistry, Faculty of Education, Alzaeim Alazhari University, Khartoum, Sudan*
[b]*Department of Chemistry, Faculty of Science, Taif University, Al-Haweiah, P.O. Box 888, 21974 Taif, Saudi Arabia*
[c]*Department of Chemistry, Faculty of Science, Port Said University, Egypt*

Received 21 January 2013; accepted 24 June 2013
Available online 10 July 2013

KEYWORDS

Quinidine;
Charge-transfer interaction;
Powder X-ray diffraction;
Morphology;
Thermal analysis

Abstract Investigation of charge-transfer (CT) complexes of drugs has been recognized as an important phenomenon in understanding of the drug–receptor binding mechanism. Structural, thermal, morphological and biological behavior of CT complexes formed between drug quinidine (Qui) as a donor and quinol (QL), picric acid (PA) or dichlorodicyanobenzoquinone (DDQ) as acceptors were reported. The newly synthesized CT complexes have been spectroscopically characterized via elemental analysis; infrared (IR), Raman, ^{1}H NMR and electronic absorption spectroscopy; powder X-ray diffraction (PXRD); thermogravimetric (TG) analysis and scanning electron microscopy (SEM). It was found that the obtained complexes are nanoscale, semi-crystalline particles, thermally stable and spontaneous. The molecular composition of the obtained complexes was determined using spectrophotometric titration method and was found to be 1:1 ratios (donor:acceptor). Finally, the biological activities of the obtained CT complexes were tested for their antibacterial activities. The results obtained herein are satisfactory for estimation of drug Qui in the pharmaceutical form.

*Corresponding author. Tel.: +249 912998623.
E-mail address: halahassan_1972@yahoo.com (H.H. Eldaroti)

Peer review under responsibility of Xi'an Jiaotong University.

Production and hosting by Elsevier

1. Introduction

Considerable attention has recently been paid to the formation of stable charge-transfer (CT) complexes that result from the reaction between acceptors and drugs or biological compounds. This interest stems from the significant physical and chemical properties of these complexes. The CT complexation is an important

2095-1779
http://dx.doi.org/10.1016/j.jpha.2013.06.003

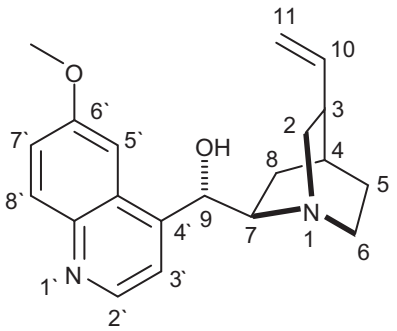

Scheme 1 Chemical structure of quinidine.

technique that is cheaper, simpler, and more efficient than the methods of drug determination described in the literature [1]. The study of the CT complexes of drugs may be useful in understanding the drug–receptor interactions and the mechanisms of drug action [2]. Furthermore, the crystalline CT complexes have a vital role in biological systems such as antimicrobial activity and DNA-binding. Literature shows that the CT complexes exhibit potential antimicrobial properties against Gram-positive and Gram-negative bacteria as well as fungi [3–9]. Herein, the CT interaction between the drug quinidine and three acceptors is reported. Quinidine (Qui; $C_{20}H_{24}N_2O_2$, Scheme 1) is a pharmaceutical agent that acts as a class I antiarrhythmic drug in the heart [10]. It is a stereoisomer of quinine, originally derived from the bark of the cinchona tree. Qui is well-known as medicinally important compound [11–15]. It is used to treat and control atrial fibrillation and atrial flutter. Qui is also approved to treat premature ventricular contractions and paroxysmal atrial tachycardia or paroxysmal atrioventricular junctional rhythm. It may also be used to treat malaria, although quinine is preferred [16,17].

To provide the basic data that can be used to understand drug–receptor mechanism, the CT complexes of Qui with quinol (QL), picric acid (PA) and dichlorodicyanobenzoquinone (DDQ) were synthesized and spectroscopically investigated. The newly synthesized CT complexes have been structurally characterized via elemental analysis; infrared (IR), Raman, ^{1}H –NMR and electronic absorption spectroscopy; powder X-ray diffraction (PXRD); and scanning electron microscopy (SEM) to interpret the behavior of the interactions. Finally, the biological activity of the CT complexes was tested for their antibacterial activities.

2. Materials and methods

2.1. Chemicals

All chemicals used were of analytical grade. Qui ((9S)-6′-methoxycinchonan-9-ol, $C_{20}H_{24}N_2O_2$; 324.417) and π-acceptors of quinol (QL) (Benzene-1,4-diol; $C_6H_6O_2$; 110.11), picric acid (PA) (2,4,6-trinitrophenol; $C_6H_3N_3O_7$; 229.1) or DDQ (2,3-dichloro-5,6-dicyano-1,4-benzoquinone; $C_8Cl_2N_2O_2$; 227) were purchased from Merck Chemical Company and were used without further purification. Commercially available spectroscopic grade solvents (BDH) were also used as received. The systematic IUPAC names of the formed CT complexes are [(Qui)(QL)] complex: 6′-methoxycinchonan-1-ium-9-ol-4-hydroxybenzenol-ate ($C_{26}H_{30}N_2O_4$; 434.527); [(Qui)(PA)] complex: 6′-methoxycinchonan-1-ium-9-ol-2,4,6-trinitrobenzeno-late ($C_{26}H_{27}N_5O_9$; 553.517); [(Qui)(DDQ)] complex: 4,5-dichloro-2-cyano-3,6-dioxocyclohexa-1,4-diene-1-carbonitrilium(9*S*)-6′-methoxycinchonan-9-olate ($C_{28}H_{24}Cl_2N_4O_4$; 551.417).

2.2. Instruments

The elemental analyses of the carbon and hydrogen contents were performed by the microanalysis facility at Cairo University, Egypt, using a Perkin-Elmer CHN 2400 (USA). The electronic absorption spectra of methanolic solutions of the donor, acceptors and resulting CT complexes were recorded over a wavelength range of 200–800 nm using a Perkin-Elmer Lambda 25 UV/vis double-beam spectrophotometer at Taif University, Saudi Arabia. The instrument was equipped with a quartz cell with a 1.0 cm path length. The mid-infrared (IR) spectra (KBr discs) within the range of 4000–400 cm^{-1} for the solid CT complexes were recorded on a Shimadzu FT-IR spectrophotometer with 30 scans at 2 cm^{-1} resolution. The Raman laser spectra of the samples were measured on a Bruker FT-Raman spectrophotometer equipped with a 50 mW laser at Taif University, Saudi Arabia. ^{1}H NMR spectra were collected by the Analytical Center at King Abdul Aziz University, Saudi Arabia, on a Bruker DRX-250 spectrometer operating at 250.13 MHz with a dual 5 mm probe head. The measurements were performed at ambient temperature using DMSO-d_6 (dimethylsulfoxide, d_6) as a solvent and tetramethylsilane (TMS) as an internal reference. The ^{1}H NMR data are expressed in parts per million (ppm) and are internally referenced to the residual proton impurity in the DMSO solvent. Thermogravimetric analysis (TG) was performed under an air atmosphere between room temperature and 800 °C at a heating rate of 10 °C/min using a Shimadzu TGA-50H thermal analyzer at the Central Lab at Ain Shams University, Egypt. The X-ray diffraction patterns for the obtained CT complexes were collected on a PANalytical X'Pert PRO X-ray powder diffractometer at the Central Lab at Ain Shams University, Egypt. The instrument was equipped with a Ge(III) monochromator, and a Cu $K\alpha_1$ X-ray source with a wavelength of 0.154056 nm was used. Scanning electron microscopy (SEM) images were collected on a Jeol JSM-6390 instrument at Taif University, Saudi Arabia. The instrument was operated at an accelerating voltage of 20 kV.

2.3. Procedures

2.3.1. Reaction procedure

The solid CT complexes of Qui with QL, PA or DDQ were prepared by mixing equimolar amounts of Qui with each acceptor in methanol (10 mL). The solutions were stirred for about 20 min, and allowed to evaporate slowly at room temperature, which resulted in the precipitation of the solid CT complexes. The resultant complexes were filtered off, washed well with little amounts of methanol, and then collected and dried under vacuum over anhydrous calcium chloride for 24 h.

2.3.2. Preparation of standard stock solutions of the donor and acceptors

Stock solutions of Qui and acceptors at a concentration of 5.0×10^{-3} M were freshly prepared before each series of measurements by dissolving precisely weighed amounts in the appropriate volume of the methanol solvent. The stock solutions were protected from light.

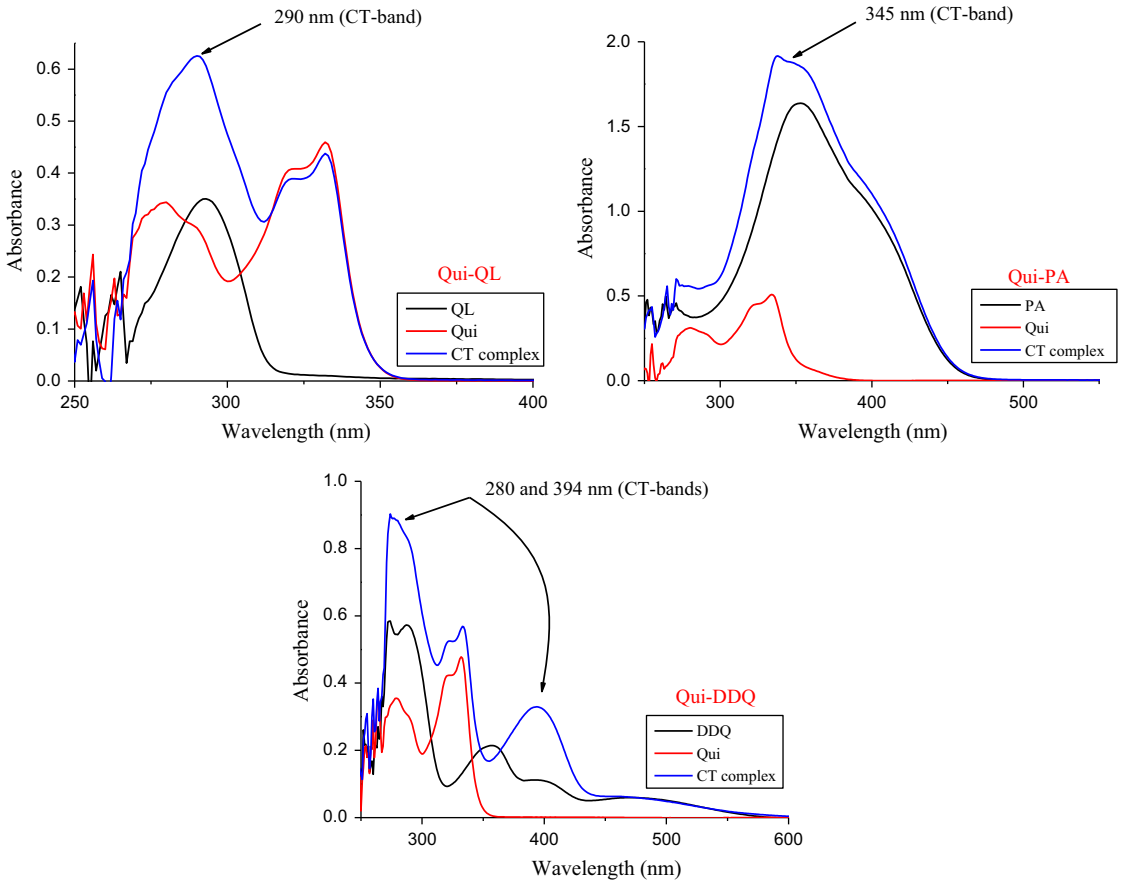

Fig. 1 Electronic absorption spectra of [(Qui)(QL)], [(Qui)(PA)] and [(Qui)(DDQ)] charge-transfer complexes in methanol solvent.

2.3.3. Spectrophotometric titration procedure

Spectrophotometric titration measurements were carried out for the reactions of Qui with QL, PA and DDQ against methanol as a blank at wavelengths of 290, 345 and 394 nm, respectively. A 0.25, 0.50, 0.75, 1.00, 1.50, 2.0, 2.50, 3.00, 3.50 or 4.00 mL aliquot of a standard solution (5.0×10^{-4} M) of the appropriate acceptor in methanol was added to 1.00 mL of 5.0×10^{-4} M Qui, which was also dissolved in methanol. The total volume of the mixture was 5 mL. The concentration of Qui (C_d) in the reaction mixture was maintained at 5.0×10^{-4} M, whereas the concentration of the acceptors (C_a) changed over a wide range of concentrations (0.25×10^{-4} M–4.00×10^{-4} M) to produce solutions with an acceptor molar ratio that varied from 4:1 to 1:4. The stoichiometry of the Qui CT complexes was obtained from the determination of the conventional spectrophotometric molar ratio according to known methods using a plot of the absorbance of each CT complex as a function of the C_d:C_a ratio. Modified Benesi–Hildebrand plots were constructed to allow the calculation of the formation constant, K_{CT}, and the absorptivity, ε_{CT}, values for each CT complex in this work.

2.3.4. Biological assessment

The antibacterial activities of the newly synthesized Qui CT complexes and the pure solvent were tested *in vitro* against two Gram-positive bacteria, *Staphylococcus aureus* (MSSA 22) and *Bacillus subtilis* (ATCC 6051), and two Gram-negative bacteria, *Escherichia coli* (K 12) and *Pseudomonas aeruginosa* (MTCC 2488), using a modified Bauer–Kirby disc diffusion method. The microanalysis facility at Cairo University, Egypt performed the investigations. For these investigations, 100 µL test bacteria were grown in 10 mL fresh medium until they reached a count of approximately 10^8 cells/mL for bacteria or 10^5 cells/mL for fungi. Then, 100 µL microbial suspension was spread onto agar plates. The nutrient agar medium for the antibacterial tests consisted of 0.5% peptone, 0.1% beef extract, 0.2% yeast extract, 0.5% NaCl and 1.5% agar-agar [18]. Isolated colonies of each strain were selected from the primary agar plates and tested for susceptibility. After the plates were incubated for 48 h at 37 °C, the inhibition (sterile) zone diameters (including the disc) were measured using slipping calipers from the National Committee for Clinical Laboratory Standards (NCCLS, 1993) [19] and are expressed in mm. The screening was performed using 100 µg/mL CT complex. An antibiotic disc of tetracycline (30 µg/disc, Hi-Media) was used as a positive control.

3. Results and discussion

3.1. Elemental analysis results

Elemental analysis (C and H) of the Qui CT complexes was performed and the obtained results are as follows: [(Qui)(QL)]: $C_{26}H_{30}N_2O_4$; Mol. wt.=434.527; Brown; Calc.: %C, 71.36; %H, 7.12; Found: %C, 71.80; %H, 6.90, [(Qui)(PA)]: $C_{26}H_{27}N_5O_9$; Mol. wt.=553.517; Pale yellow; Calc.: %C, 55.91; %H, 4.53; Found: %C, 56.37; %H, 4.88, [(Qui)(DDQ)]: $C_{28}H_{24}Cl_2N_4O_4$; Mol. wt.=551.417; Dark greenish brown; Calc.: %C, 61.54; %H, 4.52; Found: %C, 60.93; %H, 4.35. The resulting values are in good agreement with the calculated values, and the suggested

values are in agreement with the molar ratios determined from the spectrophotometric titration curves. The stoichiometry of all Qui complexes was found to be 1:1 ratios. Based on the obtained data, the formed CT complexes were formulated as [(Qui)(QL)], [(Qui)(PA)] and [(Qui)(DDQ)]. The formation of 1:1 complex was strongly supported by IR, ^{1}H NMR as well as thermal analysis.

3.2. *Electronic absorption spectra*

Fig. 1 shows the electronic spectra of Qui, acceptors and the formed CT complexes. These spectra revealed the characterization of the real absorption bands that are attributed to the CT interactions. These bands are observed at 290, 345 and (280, 394) nm for the [(Qui)(QL)], [(Qui)(PA)] and [(Qui)(DDQ)] complexes, respectively. The peak absorbance values that appeared in the spectra assigned to the formed CT complexes were measured and plotted as a function of the C_d:C_a ratio according to a known method. Spectrophotometric titration plots based on these characterized absorption bands (Fig. 2) confirmed the complex formation at a ratio (Qui: acceptor) of 1:1 in all cases. This result is strongly supported by the elemental analyses. The formation constant (K_{CT}) and the extinction coefficients (ε) of the Qui CT complexes were calculated by applying the 1:1 Benesi–Hildebrand equation in Eq. (1).

$$(C_aC_d)/A = 1/K\varepsilon + (C_a + C_d)/\varepsilon \quad (1)$$

where C_a and C_d are the initial concentrations of the electron acceptor (QL, PA or DDQ) and the electron donor (Qui), respectively, and A is the absorbance of the strongly detected CT band. Plotting the $(C_aC_d)/A$ values versus the corresponding (C_a+C_d) values for the formed Qui CT complexes, straight lines were obtained supporting our finding of the formation of 1:1 complexes. In the plots, the slope and the intercept equal $1/\varepsilon$ and $1/K\varepsilon$, respectively. The Benesi–Hildebrand plots are shown in Fig. 3, and the values of C_d, C_a, (C_d+C_a) and (C_dC_a)/A are listed in Table 1. The values of both K_{CT} and ε associated with the complexes are given in Table 2. These complexes exhibit high values for both the formation constants (K_{CT}) and the extinction coefficients (ε). The high values of K_{CT} reflect the high stabilities of the formed CT complexes as a result of the expected strong donation from the drug Qui. The equilibrium constants are strongly dependent on the nature of the used acceptor including the type of electron withdrawing substituent to it such as nitro and halo groups [20]. The data reveal that the [(Qui)(DDQ)] complex exhibits a higher K_{CT} value compared with the other two complexes, reflecting the relatively higher powerful electron acceptance ability for DDQ, which containing two cyano and two chloro groups between two carbonyl groups. The data also reveal that the [(Qui)(PA)] complex shows a higher value of ε. The ε values of Qui CT complexes in decreasing order are [(Qui)(PA)] > [(Qui)(DDQ)] > [(Qui)(QL)].

3.3. *Calculation of the spectroscopic and physical data*

The spectroscopic and physical data, such as the standard free energy (ΔG°), the oscillator strength (f), the transition dipole moment (μ), the resonance energy (R_N), and the ionization potential (I_P), were estimated for complexes dissolved in methanol at 25 °C. The oscillator strength (f) is a dimensionless quantity used to express the transition probability of the CT band. From the CT absorption spectra, the oscillator strength (f) can be estimated using the approximate formula:

$$f = 4.319 \times 10^{-9} \int \varepsilon_{CT} d\nu \quad (2)$$

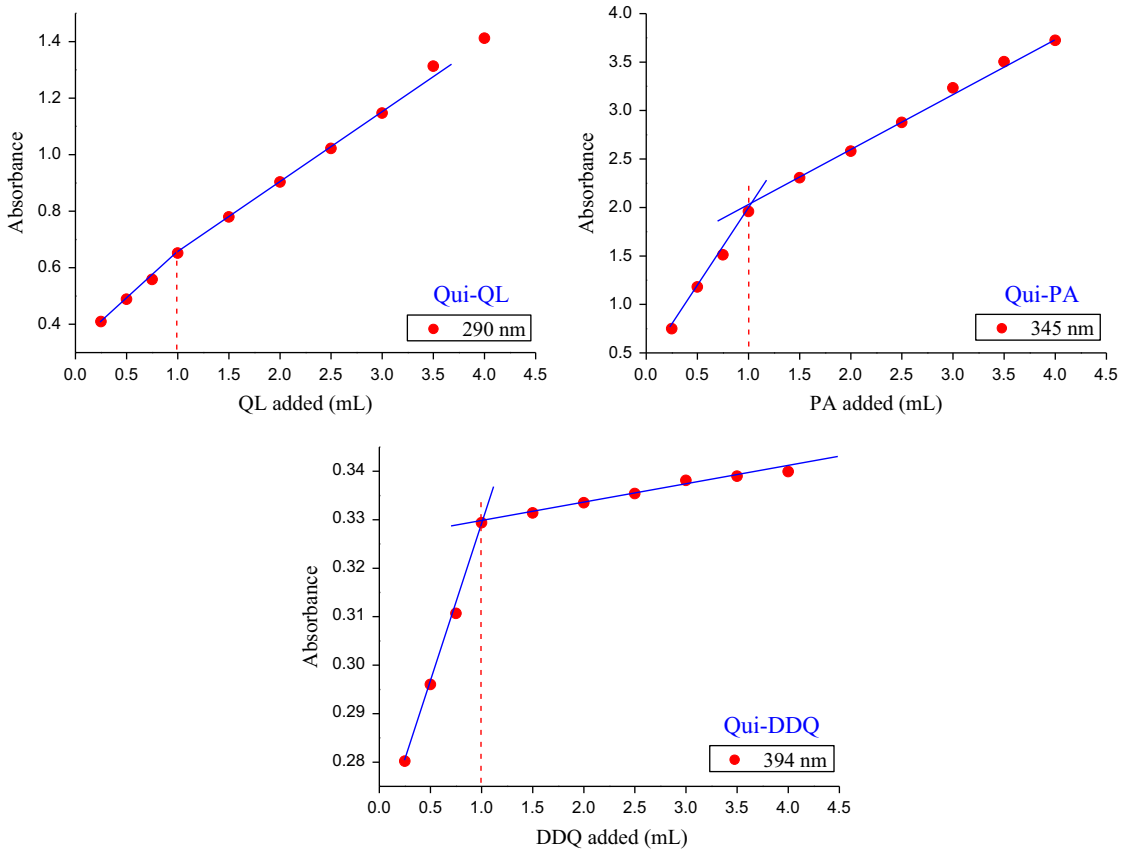

Fig. 2 Spectrophotometric titration curves for Qui charge-transfer systems in methanol solvent at the detectable peaks.

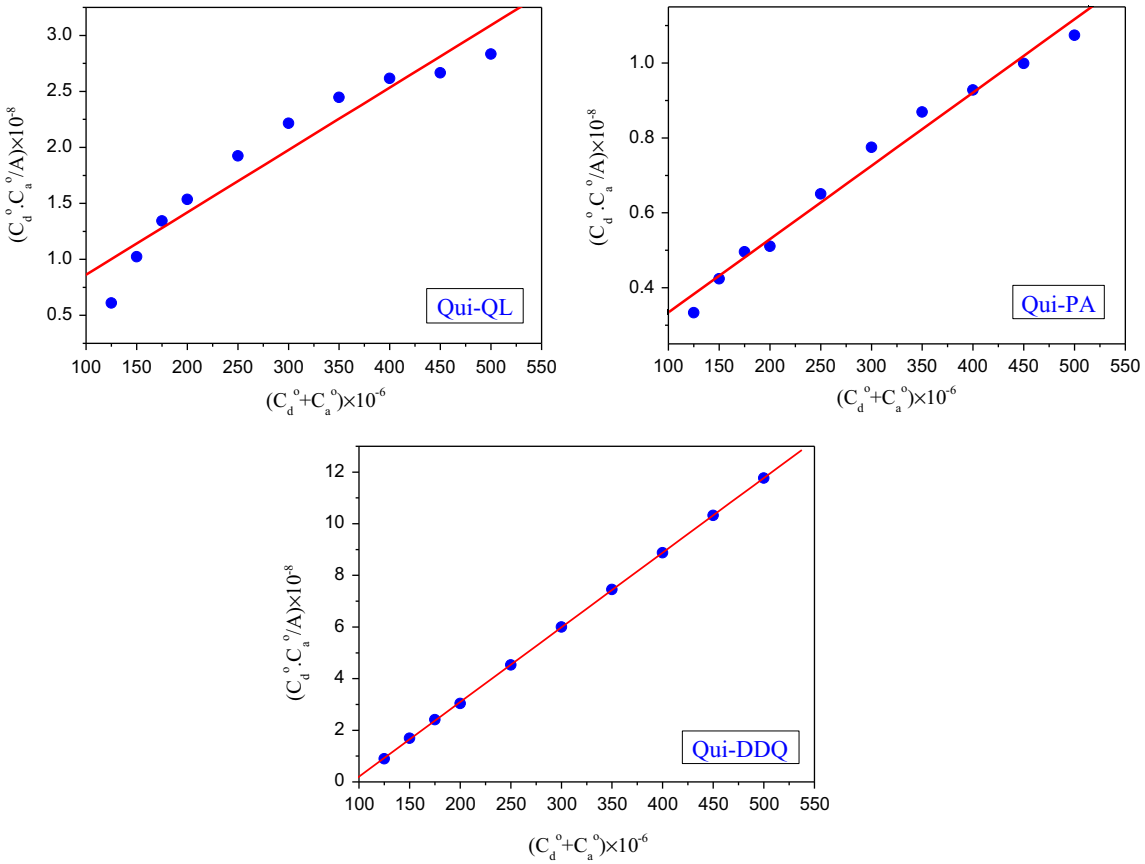

Fig. 3 The 1:1 Benesi–Hildebrand plot of Qui charge-transfer complexes in methanol solvent at the detectable peaks.

where $\int \varepsilon_{CT}\, d\nu$ is the area under the curve of the extinction coefficient of the absorption band in question plotted as a function of frequency. To a first approximation,

$$f = 4.319 \times 10^{-9} \varepsilon_{CT} \nu_{½} \tag{3}$$

where ε_{CT} is the maximum extinction coefficient of the CT band, and $\nu_{½}$ is the half-bandwidth in cm^{-1} (i.e., the bandwidth at half of the maximum extinction coefficient value). The transition dipole moments (μ) of the Qui CT complexes have been calculated from Eq. (4) [21]:

$$\mu = 0.0958\, [\varepsilon_{CT} \nu_{½} / \nu_{max}]^{½} \tag{4}$$

The transition dipole moment (μ) can be used to determine if a particular transition is allowed; the transition from a bonding π orbital to an antibonding π^* orbital is allowed because the integral that defines the transition dipole moment is nonzero. The ionization potentials (I_P) of the Qui donor in the CT complexes were calculated using the empirical equation derived by Aloisi and Pignataro represented in Eq. (5):

$$I_P(eV) = 5.76 + 1.53 \times 10^{-4} \nu_{CT} \tag{5}$$

where ν_{CT} is the wavenumber in cm^{-1} that corresponds to the CT band formed from the interaction between the donor and the acceptor. The electron-donating power of a donor molecule is measured by its ionization potential, which is the energy required to remove an electron from the highest occupied molecular orbital. Briegleb and Czekalla theoretically derived the following relationship to obtain the resonance energy (R_N):

$$\varepsilon_{CT} = 7.7 \times 10^{-4} / [h\nu_{CT} / [R_N] - 3.5] \tag{6}$$

where ε_{CT} is the extinction coefficient of the CT complex at the maximum of the CT absorption, ν_{CT} is the frequency of the CT peak, and R_N is the resonance energy of the complex in the ground state, which contributes to the stability constant of the complex (a ground-state property). The energy values (E_{CT}) of the $n \rightarrow \pi^*$ and π–π^* interactions between the Qui donor and the acceptors were calculated using the equation derived by Briegleb:

$$E_{CT} = (h\nu_{CT}) = (1243.667 / \lambda_{CT}) \tag{7}$$

where λ_{CT} is the wavelength of the CT band. The standard free energy of complexation (ΔG°) for each complex was calculated from the formation constants using the equation:

$$\Delta G^\circ = -2.303 RT \log K_{CT} \tag{8}$$

where ΔG° is the standard free energy change of the CT complexes (kJ/mol), R is the gas constant (8.314 J/mol K), T is the absolute temperature in K, and K_{CT} is the formation constant of the complex (L/mol) at room temperature.

The calculated spectroscopic and physical values for the Qui CT complexes using these Eqs. (2)–(8) are presented in Table 2. The [(Qui)(DDQ)] complex exhibits considerably higher value of oscillator strength (f), indicating a strong interaction between the drug Qui and the DDQ acceptor. DDQ is a strong electron acceptor to form stable CT complexes with the donors. The calculated ionization potential (I_P) value for the highest filled molecular orbital that participates in the CT interaction of the Qui donor is approximately 10.29. The obtained values of standard free energy change (ΔG°) for the [(Qui)(QL)], [(Qui)(PA)] and [(Qui)(DDQ)] are −35.722, −35.102 and −34.414 kJ/mol, respectively;

Table 1 The values of C_d, C_a, C_d+C_a and C_dC_d/A for the Qui CT complexes.

Ratio (A:D)	C_d ($\times 10^{-4}$)	C_a ($\times 10^{-4}$)	C_d+C_a ($\times 10^{-6}$)	C_dC_d/A ($\times 10^{-8}$)	Qui–QL complex		Qui–PA complex		Qui–DDQ complex	
					Abs. 290 nm	C_dC_a /A ($\times 10^{-8}$)	Abs. 345 nm	C_dC_a /A ($\times 10^{-8}$)	Abs. 394 nm	C_dC_a /A ($\times 10^{-8}$)
0.25	1.00	0.25	125	0.25	0.4095	0.6105	0.7500	0.3333	0.2802	0.8922
0.50	1.00	0.50	150	0.50	0.4887	1.0231	1.1794	0.4239	0.2960	1.6892
0.75	1.00	0.75	175	0.75	0.5585	1.3429	1.5122	0.4960	0.3107	2.4139
1.00	1.00	1.00	200	1.00	0.6516	1.5347	1.9579	0.5108	0.3294	3.0358
1.50	1.00	1.50	250	1.50	0.7795	1.9243	2.3066	0.6503	0.3314	4.5263
2.00	1.00	2.00	300	2.00	0.9031	2.2146	2.5800	0.7752	0.3335	5.9970
2.50	1.00	2.50	350	2.50	1.0218	2.4467	2.8770	0.8690	0.3354	7.4538
3.00	1.00	3.00	400	3.00	1.1470	2.6155	3.2330	0.9279	0.3381	8.8731
3.50	1.00	3.50	450	3.50	1.3127	2.6663	3.5035	0.9990	0.3390	10.325
4.00	1.00	4.00	500	4.00	1.4114	2.8341	3.7241	1.0741	0.3399	11.768

these negative values indicate that the interaction between the Qui and the acceptors is spontaneous [22,23].

3.4. *Interpretation of IR and Raman spectra*

The IR absorption spectra of the Qui solid CT complexes were registered in the frequency range of 4000–400 cm^{-1} using KBr disc and their peak assignments for the important characteristic bands are given in Table 3. The full IR and Raman spectra of the Qui CT complexes are shown in Figs. 4 and 5, respectively. The IR spectra of the [(Qui)(QL)] and [(Qui)(PA)] complexes are characterized by a broad strong-to-medium band that appears at 2872 cm^{-1} for the QL complex and at 2820 cm^{-1} for the PA complex, which does not appear in the spectra of the free Qui donor or those of the QL and PA acceptors. These broadened peaks are attributed to the stretching vibration of the intermolecular hydrogen bond formed through the transfer of proton from the acidic center on the QL and PA acceptors to the basic center of the Qui donor (lone pair of electrons on the N (1) atom) to form $^{+}$NH based on acid–base theory [24–29].

The IR and Raman spectra of the [(Qui)(DDQ)] complex indicated that the band that results from the ν(C≡N) vibration of the free DDQ acceptor changed in frequency and decreased in intensity in the complexes upon CT complexation. Free DDQ shows two ν(C≡N) vibration at 2250 and 2231 cm^{-1}, while in its complex; ν(C≡N) occurs at lower wavenumber values (IR/Raman; 2209/2225 cm^{-1}). It is clear that ν(C≡N) of DDQ is decreased upon complexation. The characteristic band of ν(OH) group observed at 2955 cm^{-1} in the free Qui donor, is shifted in the complex and its intensity is affected. The group of bands assigned to ν(C–Cl) vibrations, which appeared at 893 and 800 cm^{-1} in the free DDQ, exhibited a shift to lower wavenumbers at 862 and 780 cm^{-1} and decreasing in the intensities of the characteristic peaks. These observations clearly confirm that the (–OH) group in the Qui donor and the (–C≡N) group in the DDQ acceptor participated in the complexation process. Because DDQ lacks acidic centers, the molecular complex can be concluded to form through $\pi \rightarrow \pi^*$ and/or $n \rightarrow \pi^*$ charge migration from the HOMO of the donor to the LUMO of the acceptor. The $\pi \rightarrow \pi^*$ CT complex is formed via the benzene ring (electron-rich group) of the Qui and DDQ reagents (electron acceptor) [30]. The cyano group (–C≡N) is an electron-withdrawing group that exists in DDQ in a conjugated bonding system. The 2CN groups in DDQ withdraw electrons from the aromatic ring, and such a process will make the aromatic ring an electron-accepting region. The π^*–CN electron density appears to increase and more easily accept a proton from the donor because of the electron-withdrawing process and the conjugated electron system. So, the interaction mode between Qui and the DDQ acceptor also occurs through the migration of a H^+ ion to one of the cyano groups in the DDQ acceptor to form a positive ion (–C≡N$^+$H) that associates with the (–O$^-$) anion to form ion pairs [31,32].

3.5. *Interpretation of ^{1}H NMR spectra*

The nuclear magnetic resonance spectra present the persuasive confirmation of the complexation pathway. Thus, the 400 MHz ^{1}H NMR spectra of the Qui CT complexes were measured in DMSO-d_6 at room temperature and are given in Fig. 6. The chemical shifts (δ) of the different types of protons of the CT complexes are [(Qui)(QL)] complex: δ=1.32–1.37 (m, 5H, 2(C**H**$_2$)) at C(5), C(8) and

Table 2 Spectroscopic and physical data of the Qui CT complexes.

Complex	λ_{max} (nm)	E_{CT} (eV)	K_{CT} (L/mol)	ε_{max} (L/mol/cm)	f	μ	I_p	R_N	ΔG° (25 °C) (kJ/mol)
[(Qui)(QL)]	290	4.29	1.83×10^4	1.80×10^4	15.51	30.92	11.04	1.21	−35.7
[(Qui)(PA)]	345	3.60	1.42×10^4	5.10×10^4	22.03	40.20	10.20	1.03	−35.1
[(Qui)(DDQ)]	394	3.16	2.07×10^4	3.47×10^4	37.32	17.68	9.64	0.85	−34.4

Table 3 Infrared frequencies[a] (cm^{-1}) and tentative assignments for Qui, acceptors and the formed CT complexes.

Qui	QL	PA	DDQ	[(Qui)(acceptor)] CT complexes			Assignments[b]
				QL	PA	DDQ	
3070 mw	3262 br	3416 br	3325 w	3658 w	3053 w	3195 s, br	ν(N–H)
2955 vs	3031 m	3103 ms	3218 br	3152 s, br	2976 m	3009 w	ν(O–H)
				3077 m		2949 s	ν(C–H); aromatic
							ν(+NH)
2854 vs, sh	2857 m	2980 sh	2250 vw	2938 vs	2880 mw	2209 ms	ν_s(C–H)+ν_{as}(C–H)
2723 m, br		2872 w	2231 ms	2872 s, sh	2820 m, br		Hydrogen bonding
							ν(C≡N); DDQ
1621 ms	1518 vs	1632 vs	1673 vs	1622 s	1613 vs	1622 s	δ_{def}(N–H); Qui, complex
1590 m		1608 vs	1552 vs	1591 m, sh	1566 s	1562 s	$\nu_{as}(NO_2)$; PA, complex
1510 s		1529 vs		1510 vs	1545 s, sh	1511 s	ν(C=O)+ν(C=C)+ν(C–N)
					1519 ms		δ(C–H) deformation
1466 s	1477 vs	1432 s	1451 s	1468 m	1430 ms	1454 vs, sh	ν(C=N); Qui, complex
				1433 m, sh		1435 vs	ν(C=C) (in-ring), aromatic
1263 s	1366 ms	1343 ms	1358 w	1363 m	1365 s	1265 m, sh	ν(C–C)+ν(C–O)+ν_s(C–N)
1188 m	1244 vs	1150 ms	1267 s	1329 mw	1321 vs	1240 vs	C–H in-plane bending
1106 m	1222 vs	1086 s	1172 vs	1239 vs	1268 s	1080 ms	$\nu_s NO_2$; PA, complex
1076 m	1210 vs		1072 w	1028 s	1245 m, sh	1029 ms	
1051 ms	1164 ms		1010 vw	998 m	1164 m	989 mw	
1020 m	1097 m				1033 m		
857 ms	827 s	917 vs	893 s	916 m	917 ms	888 m	δ_{rock}, NH
821 ms	759 vs	781 s	800 vs	836 s	865 m	862 m	ν(C–Cl); DDQ, complex
715 m	616 m	732 s	720 s	763 m	838 m, sh	780 w	C–H out of plane bending
857 ms	525 ms	703 s	615 ms	718 m	790 m	718 mw,m	Skeletal vibrations
821 ms		652 sh	457 ms		712 s		CNC deformation
715 m		522 ms					δ(ONO); PA, complex

[a] s, strong; w, weak; m, medium; sh, shoulder; v, very; vs, very strong; br, broad.
[b] ν, stretching; ν_s, symmetrical stretching; ν_{as}, asymmetrical stretching; δ, bending.

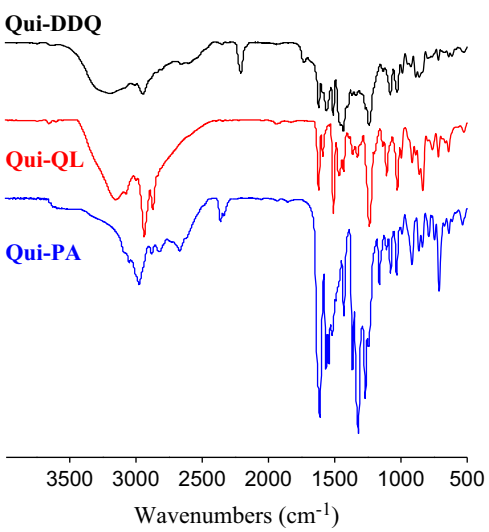

Fig. 4 Infrared spectra of Qui charge-transfer complexes.

1H at C(4)), 2.69–2.75 (t, 2H, CH_2 at C(7)), 2.93–3.04 (m, 1H, CH at C(3)), 3.17–3.18 (d, 2H, J=4.8 Hz, CH_2 at C(2)), 3.89 (s, 3H, OC**H**$_3$), 4.1–4.12 (m, 1H, CH at C(6)), 5.04–5.07 (2 dd appears m, 2H, =C**H**$_2$ at C(10)), 5.10 (s, 1H, OH at C(11)), 5.26–5.29 (m, 1H, C**H**=at C(9)), 5.63 (d, 2H, J=4.8 Hz, phenolic protons at C(1,2 quinol ring)), 6.05–6.14 (b, 1H, NH^+ Hydrogen bonded), 7.37 (d, 2H, J=2.8 Hz, phenolic protons at C(3,4 quinol ring)), 7.37 (s, 1H, CH, at C(5′) quinoline ring), 7.39 (d, 1H, J=2.4 Hz, CH, at C(7′) quinoline ring), 7.46 (d, 1H, J=2.4 Hz, CH, at C(3′) quinoline ring), 7.49 (d, 1H, J=4.4 Hz, CH, at C(8′) quinoline ring), 7.91 (d, 1H, J=9.2 Hz, CH, at C(2′) quinoline ring), 8.67 (s, 1H, OH, quinol); [(Qui)(PA)] complex: δ=1.16–1.18 (m, 1H, CH at C(4)), 1.81–1.95 (m, 4H, 2(C**H**$_2$) at C(5), C(8)), 2.66–2.68 (t, 2H, CH_2 at C(7)), 3.25–3.30 (m, 1H, CH at C(3)), 3.46–3.48 (d, 2H, J=10.4 Hz, CH_2 at C(2)), 3.96 (s, 3H, OC**H**$_3$), 4.00 (m, 1H, CH at C(6)), 5.21–5.26 (2 dd appears m, 2H, =C**H**$_2$ at C(10)), 5.94 (s, 1H, OH at C(11)), 6.01–6.10 (m, 1H, C**H**=at C(9)), 6.50 (s, 1H, NH^+ Hydrogen bonded), 7.31 (s, 1H, CH, at C(5′) quinoline ring), 7.45 (d, 1H, J=2.4 Hz, CH, at C(7′) quinoline ring), 7.48 (d, 1H, J=2.4 Hz, CH, at C(3′) quinoline ring), 7.62

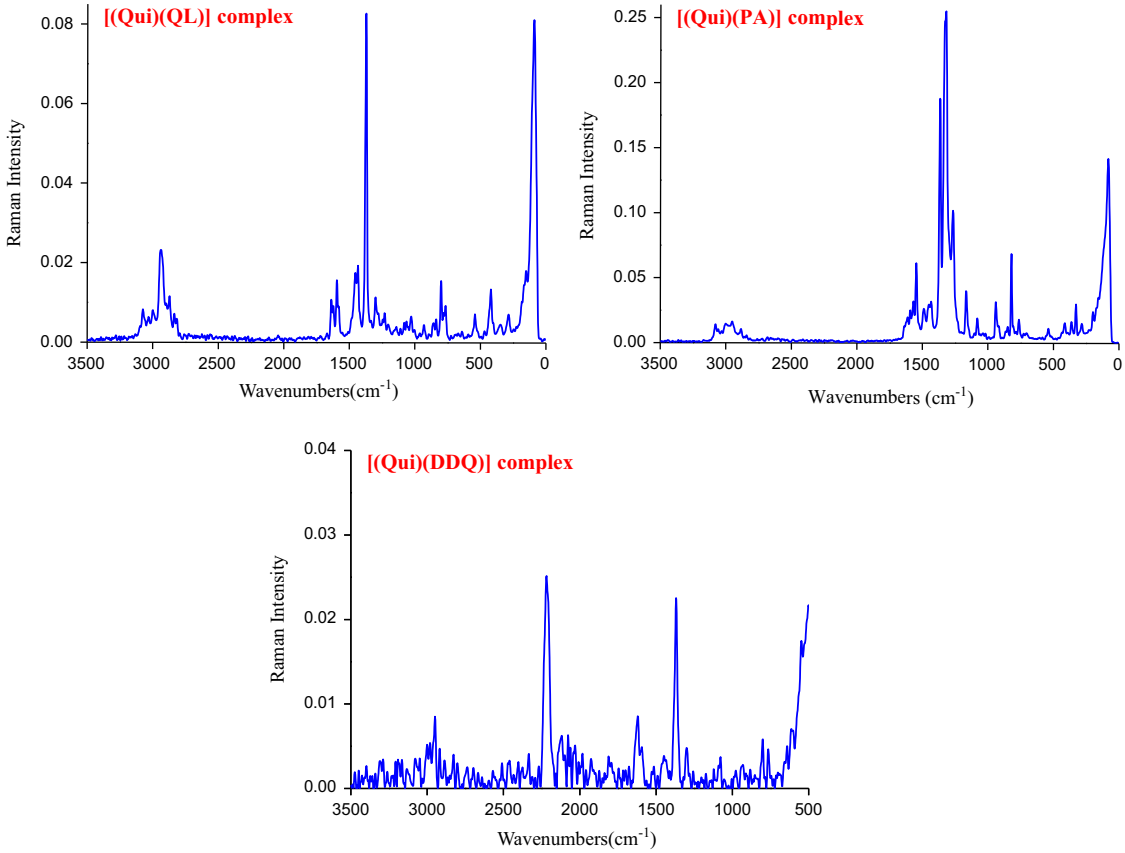

Fig. 5 Raman spectra of Qui charge-transfer complexes.

(d, 1H, J=4.8 Hz, CH, at C(8′) quinoline ring), 7.98 (d, 1H, J=9.2 Hz, CH, at C(2′) quinoline ring), 8.58 (s, 2H, picrate protons); [(Qui)(DDQ)] complex: δ=1.14 (m, 1H, CH at C(4)), 1.79–1.93 (m, 4H, 2(C**H**$_2$) at C(5), C(8)), 2.65–2.67 (t, 2H, CH_2 at C(7)), 3.22–3.27 (m, 1H, CH at C(3)), 3.42–3.43 (d, 2H, J=2.8 Hz, CH_2 at C(2)), 3.99 (m, 4H, OC**H**$_3$, 1H, CH at C(6)), 5.21–5.25 (2 dd appears m, 2H, =C**H**$_2$ at C(10)), 6.01–6.10 (m, 1H, C**H**= at C(9)), 6.21 (s, 1H, NH^+), 7.43 (d, 1H, J=8.8 Hz, CH, at C(7′) quinoline ring), 7.49 (s, 1H, CH, at C(5′) quinoline ring), 7.62 (d, 1H, J=4.4 Hz, CH, at C(3′) quinoline ring), 7.96 (d, 1H, J=9.2 Hz, CH, at C(8′) quinoline ring), 8.75 (d, 1H, J=4.4 Hz, CH, at C (2′) quinoline ring).

In the [(Qui)(QL)] complex, the phenolic proton (–OH) signal, which is observed at approximately δ~8.59 ppm in the spectrum of the QL acceptor [29], decreased in intensity with a downfield shift for the non-hydrogen-bonded one (8.67 ppm) in the spectrum of the CT complex due to deprotonation from acceptor-to-donor. Besides, the appearance of the characteristic broad band at 6.05–6.14 ppm, which is attributed to the formation of ($^+$NH), indicates the involvement of the N (1) atom of Qui donor and (–OH) group of QL acceptor in chelating through the deprotonation from the QL acceptor to the Qui donor. The intensities and chemical shifts of the aromatic signals were significantly affected by the existence of the (N^+–H) charge-transfer interaction between the donor and acceptor molecules. In the [(Qui)(PA)] complex, it is clearly obvious that, the peak at δ=11.94 ppm, which is assigned to the (–OH) proton of the free picric acid acceptor, was absent in the spectrum of this complex, which is attributed to the formation of the CT complex. Instead, a new peak is observed at 6.50 ppm in the complex, which is not detected in the spectrum of the free donor, attributing to the proton of ($^+$NH). Together, these data confirm the formation of intermolecular hydrogen bond between PA and Qui [33]. The characteristic signals presences within the range of 7.31–7.98 ppm were assigned to the protons (CH) of quinoline ring. It is clearly obvious in [(Qui)(DDQ)] complex that, the new signal observed at 6.21 in the spectrum of this complex, which is attributed to the proton of ($^+$NH), confirms that the (–OH) and (–C≡N) groups are primarily involved in the formation of the CT complex between Qui and DDQ. The migration of the H^+ ion from the (–OH) group in the Qui donor to one of the two cyano groups in the DDQ acceptor resulted in the formation of a positive ion (–C≡N^+H), which is associated with the anion O^-; this result is also confirmed from the disappearance of the (–OH) signal in the spectrum of CT complex.

3.6. *Thermal results*

The thermogravimetric analysis (TG) provided information about the thermal stabilities of the prepared CT complexes and about the differences in the physical behavior of the starting and resulting compounds. In order to verify CT interaction between Qui donor and acceptors and thermal stability of the new CT complexes, the thermogravimetric analysis of the Qui CT complexes was carried out over the temperature range of 25–800 °C under an air atmosphere using 6.83, 8.30 and 11.50 mg samples for [(Qui)(QL)], [(Qui)(PA)] and [(Qui)(DDQ)] complexes, respectively. The TG curves were redrawn as mg mass loss versus temperature. Fig. 7 shows the thermograms for Qui CT complexes and thermal

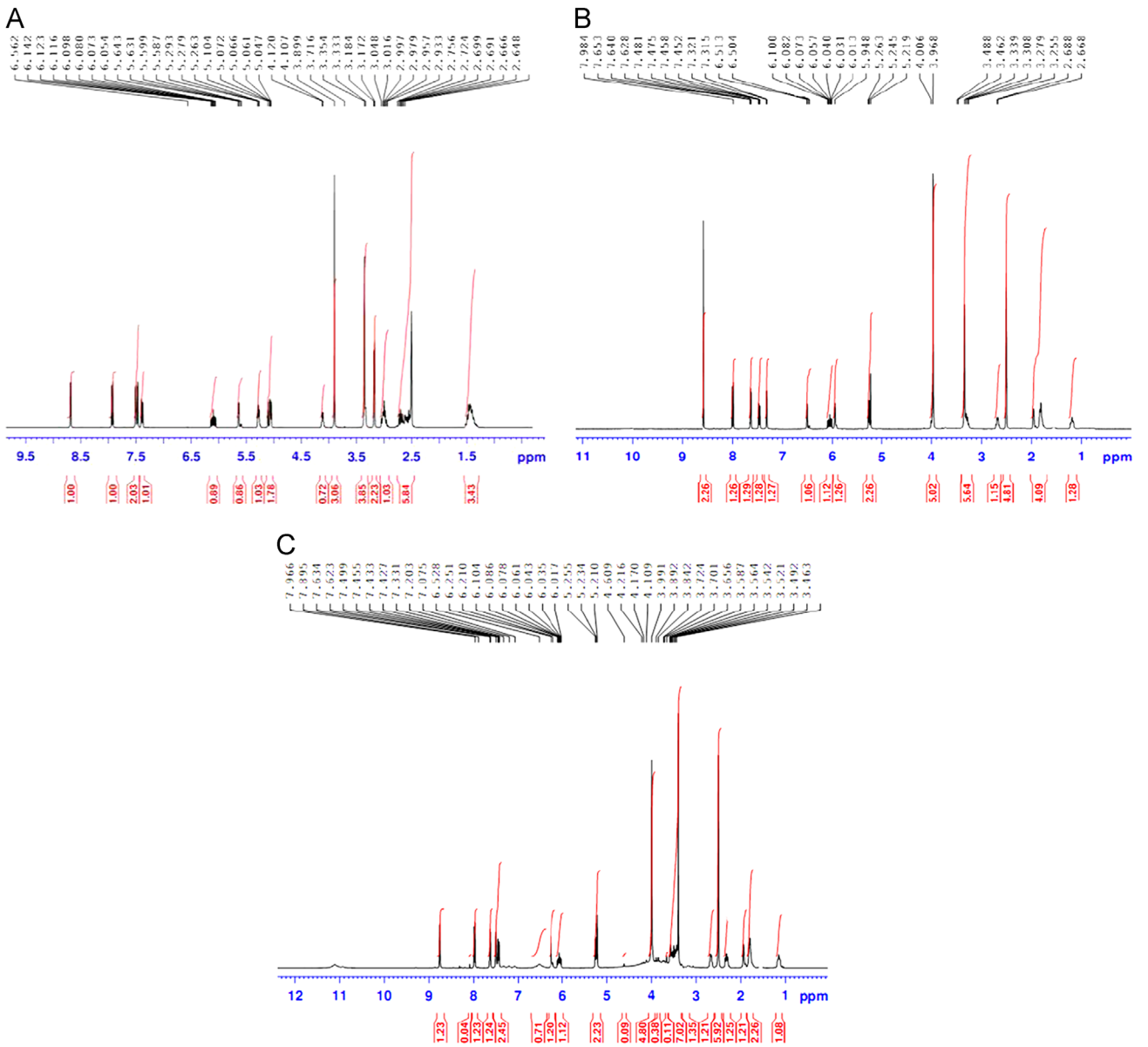

Fig. 6 ^{1}H NMR spectra of (A) [(Qui)(QL)], (B) [(Qui)(PA)] and (C) [(Qui)(DDQ)] complexes.

analyses data are listed in Table 4. The overall loss of mass from the TG curves is 95.31% for [(Qui)(QL)], 93.45% for [(Qui)(PA)] and 65.45% for [(Qui)(DDQ)] complex.

The obtained data indicate that the [(Qui)(QL)] complex is thermally stable in the range of 25–333 °C. Decomposition of the complex began at ~333 °C and finished at ~655 °C. The thermal decomposition of this complex occurs completely in two-steps within the range of 25–800 °C. The first mass loss step occurred between 25 and 333 °C and is corresponded to the loss of $5C_2H_2$, $2NO_2$ and $5CO_2$ molecules with a weight loss of 64.96% very close to the expected theoretical value of 64.90%. The second degradation step at 333–800 °C is attributed to the loss of $4C_2H_2$, CO_2 and $6H_2$ molecules, representing a weight loss of (obs.=30.35, cal.= 29.46%) with a few carbon atoms remaining as a residual. The thermal analysis curve of [(Qui)(PA)] complex indicates that decomposition takes place in two clear decomposition steps within the 25–800 °C temperature range. The first decomposition step within the temperature range 25–308 °C has a weight loss of about 57.21%, and is attributed to the loss of $4C_2H_2$, $3NO_2$ and $2CO_2$ molecules. The second decomposition step existed within the 308–800 °C temperature range, which is assigned by the removal of $6C_2H_2$, NO_2, CO_2, NH_3 and $2H_2$ molecules with some carbon atoms remaining as final fragment. This step is associated with a total weight loss of 36.24%, which is in good agreement with the calculated value (36.67%). The [(Qui)(DDQ)] complex began decomposing at ~227 °C in three clear decomposition steps within the 25–800 °C temperature range. The first decomposition step within the temperature range 25–227 °C corresponds to loss of 2HCN molecules representing a weight loss of 10.53%, which is in good agreement with the calculated value (9.79%). The second decomposition step found within the temperature range of 227–397 °C which is assigned by the removal of Cl_2 and $2CO_2$ molecules represents a weight loss of 19.93% very close to the expected theoretical value of 20.13%. The last decomposition step

has a weight loss of about 34.99%, which is reasonably by the loss of $3C_2H_2$, $2CO_2$, $2NH_3$ and $5H_2$ molecules. The decomposition of this complex ended with carbon atoms as a final residual.

3.7. Kinetic results

In recent years, there has been increasing interest in determining the rate-dependent parameters of solid-state non-isothermal decomposition reactions by analysis of TG curves. Several equations have been proposed as means of analyzing a TG curve and obtaining values for kinetic parameters. Two major different methods were used to evaluate the kinetic thermodynamic parameters: the Coats–Redfern method and the Horowitz–Metzger method.

The Coats–Redfern equation (Eq. (9)), which is an atypical integral method, can be represented as

$$\int_{0\to\infty} d\alpha/(1-\alpha)^n = (A/\varphi)\int_{T1\to T2} e^{-E^*/RT}\,dT \tag{9}$$

For convenience of integration, the lower limit T_1 is usually taken as zero. After integration, this equation can be represented as

$$\mathrm{Ln}[-\ln(1-\alpha)/T^2] = -E^*/RT + \ln[AR/\varphi E^*] \tag{10}$$

where α is the fraction of the sample decomposed at time t, T is the derivative peak temperature, A is the frequency factor, R is the gas constant, E^* is the activation energy, and φ is the linear heating rate.

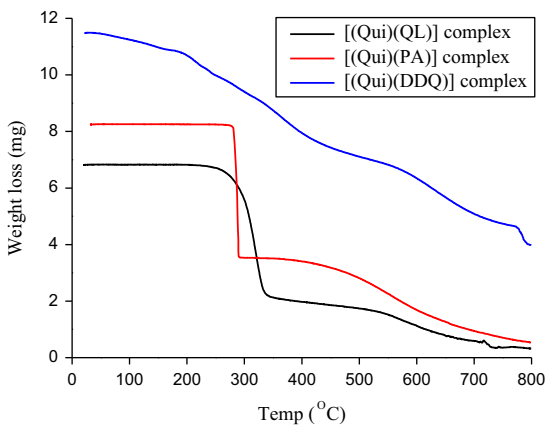

Fig. 7 TG curves of Qui charge-transfer complexes.

A plot of the left-hand side (LHS) against $1/T$ was constructed and was found to be linear. E^* is the energy of activation in kJ/mol and was calculated from the slope. The A (s^{-1}) value was calculated from the intercept. The entropy of activation, ΔS^* (J/K mol) was calculated using the equation

$$\Delta S^* = R\,ln(Ah/kT_s) \tag{11}$$

where k is the Boltzmann constant, h is Planck's constant, and T_s is the DTG peak temperature.

The Horowitz–Metzger equation (Eq. (12)) was written in the following form:

$$\log[\log(w_\alpha/w_\gamma)] = E^*\theta/2.303RT_s^2 - \log 2.303 \tag{12}$$

where $\theta = T - T_s$, $w_\gamma = w_\alpha - w$, w_α is the mass loss at the completion of the reaction, and w is the mass loss at time t.

The plot of $\log[\log(w_\alpha/w_\gamma)]$ versus θ was constructed and was observed to be linear, and E^* was calculated from its slope. The pre-exponential factor, A, was calculated from Eq. (13):

$$E^*\theta/RT_s^2 = A/[\varphi \exp(-E^*/RT_s)] \tag{13}$$

From the TG curves, the activation energy, E^*, the entropy of activation, ΔS^*, the enthalpy of activation, ΔH^*, and the Gibbs free energy, ΔG^*, were calculated from

$$\Delta H^* = E^* - RT \qquad \text{and} \qquad \Delta G^* = \Delta H^* - T\Delta S^*$$

The kinetic thermodynamic parameters for the decomposition of the Qui CT complexes; the activation energy (E^*), the frequency factor (A), the enthalpy of activation (H^*), the entropy of activation (S^*) and the free energy of activation (G^*) were evaluated graphically (Fig. 8) by employing the Coats–Redfern and Horowitz–Metzger methods, and the evaluated data are listed in Table 5. The kinetic data obtained from the two methods are comparable and in agreement with each other. The activation energy (E^*) of the complexes is expected to increase with increasing thermal stability of complexes. Hence, the E^* value for [(Qui)(DDQ)] complex exhibits a higher activation energy value than other complexes, which indicates the higher thermal stability of the [(Qui)(DDQ)] complex. Comparing the E^* values for the main decomposition stage of the Qui CT complexes gave the order DDQ > PA > QL for the different acceptors. These differences may be caused by the reactivity of the complexes

Table 4 Thermal decomposition data for the Qui CT complexes.

Complex	Stage	TG range (°C)	Weight loss (%)		Evolved moiety
			Found	Calculated	
[(Qui)(QL)] $C_{26}H_{30}N_2O_4$	I	25–333	64.96	64.90	$5C_2H_2+2NO_2+5CO_2$
	II	333–800	30.35	29.46	$4C_2H_2+CO_2+6H_2$
	Residue	–	4.69	5.52	Residual carbon
[(Qui)(PA)] $C_{26}H_{27}N_5O_9$	I	25–308	57.21	56.73	$4C_2H_2+3NO_2+2CO_2$
	II	308–800	36.24	36.67	$6C_2H_2+NO_2+CO_2+NH_3+2H_2$
	Residue	–	6.55	6.50	Residual carbon
[(Qui)(DDQ)] $C_{28}H_{24}Cl_2N_4O_4$	I	25–227	10.53	9.79	2HCN
	II	227–397	19.93	20.13	Cl_2+2CO_2
	III	397–800	34.99	35.18	$3C_2H_2+2CO_2+2NH_3+5H_2$
	Residue	–	34.55	34.82	Residual carbon

and the electronic configuration of the acceptor when attached to Qui donor. The calculated E^* values using the Coats–Redfern and Horowitz–Metzger methods for the main decomposition stage of the complexes are found to be 8.58×10^4 kJ/mol for [(Qui)(QL)], 9.13×10^4 kJ/mol for [(Qui)(PA)] and 9.68×10^4 kJ/mol for [(Qui)(DDQ)] complex. The entropy of activation (ΔS^*) is found to be of negative values in all the CT complexes which indicate that the decomposition reactions proceed spontaneously. The ΔS^* values of the Qui CT complexes arranged in decreasing order are [(Qui)(PA)] > [(Qui)(DDQ)] > [(Qui)(QL)]. The satisfactory values for the correlation coefficients (r) from the Arrhenius plots of the thermal decomposition steps were observed to be ~1 in all cases, which indicates a good fit with the linear function and reasonable agreement between the experimental data and the kinetic parameters.

3.8. *Structural interpretation*

The structures of the complexes of drug Qui with QL, PA or DDQ acceptor are confirmed by the elemental analysis, spectrophotometric titration, IR and ^{1}H NMR spectra, and thermal analysis data. The suggested structures of the CT complexes are given as shown in Schemes 2–4.

3.9. *Powder X-ray diffraction characterization*

Powder X-ray diffraction (PXRD) studies were carried out for the [(Qui)(QL)] and [(Qui)(PA)] complexes to demonstrate the crystallinity using PANalytical model X'PERT-PRO X-ray powder diffractometer system. The indexed X-ray diffraction patterns in

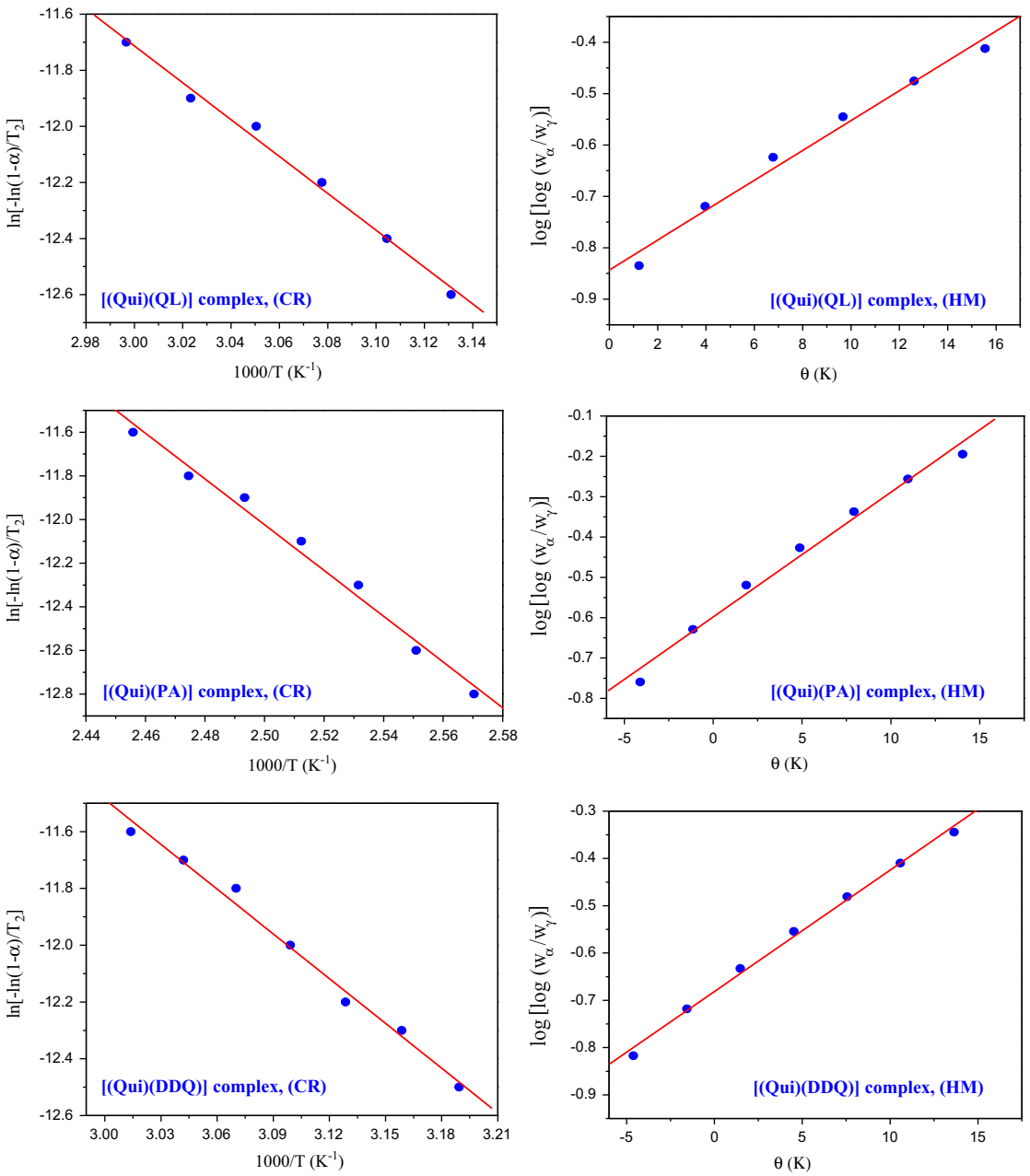

Fig. 8 Kinetic curves for Qui charge-transfer complexes (CR: Coats–Redfern equation, HM Horowitz–Metzger equation).

Table 5 Kinetic parameters determined using the Coats–Redfern (CR) and Horowitz–Metzger (HM).

Complex	Stage	Method	Parameters					r
			E (kJ/mol)	A (s^{-1})	ΔS (J/mol K)	ΔH (kJ/mol)	ΔG (kJ/mol)	
[(Qui)(QL)]	1st	CR	8.48×10^4	4.98×10^6	-1.27×10^2	5.20×10^4	8.98×10^4	0.99680
		HM	8.68×10^4	2.91×10^7	-1.82×10^2	5.87×10^4	8.68×10^4	0.99080
[(Qui)(PA)]	1st	CR	8.79×10^4	3.83×10^9	-6.38×10	8.89×10^4	1.68×10^4	0.98578
		HM	9.46×10^4	2.68×10^{10}	-4.98×10	8.88×10^4	1.07×10^4	0.99060
[(Qui)(DDQ)]	1st	CR	9.37×10^4	1.57×10^4	-1.80×10^2	4.41×10^4	8.87×10^4	0.99130
		HM	9.98×10^4	2.49×10^6	-1.28×10^2	4.81×10^4	8.66×10^4	0.99830

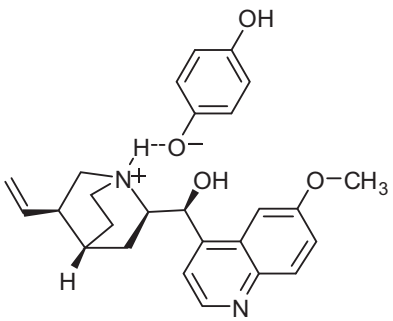

Scheme 2 Suggested structural formula of [(Qui)(QL)] complex.

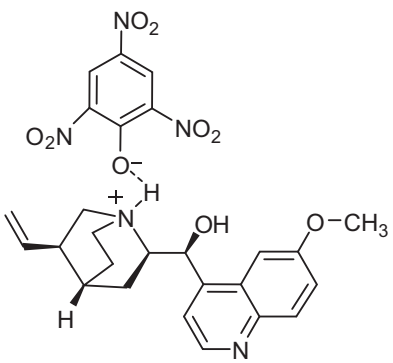

Scheme 3 Suggested structural formula of [(Qui)(PA)] complex.

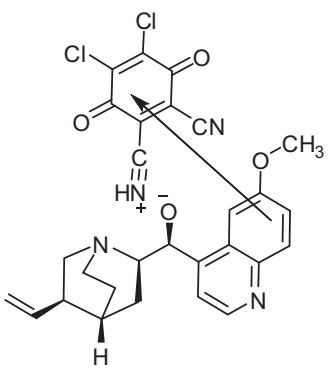

Scheme 4 Suggested structural formula of [(Qui)(DDQ)] complex.

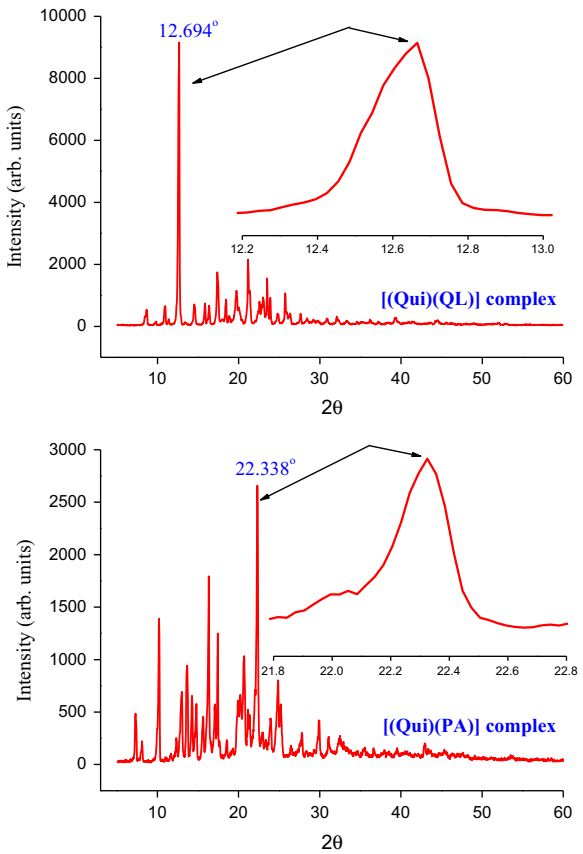

Fig. 9 X-ray diffraction pattern for [(Qui)(QL)] and [(Qui)(PA)] complexes.

the range of $5^\circ < 2\theta < 60^\circ$ for these two complexes are shown in Fig. 9. The particle size of these two complexes was estimated from their PXRD patterns based on the highest intensity value compared with the other peaks using the well-known Debye–Scherrer formula given in Eq. (14) [34]:

$$D = K\lambda/\beta\cos\theta \tag{14}$$

where D is the apparent particle size of the grains, K is a constant (0.94 for Cu grid), λ is the X-ray wavelength used (1.5406 Å), θ is half the scattering angle (the Bragg diffraction angle), and β is the full-width at half-maximum (FWHM) of the X-ray diffraction line (additional peak broadening) in radians. Table 6 presents the PXRD spectral data for the [(Qui)(QL)] and [(Qui)(PA)] complexes,

Table 6 PXRD spectral data of [(Qui)(QL)] and [(Qui)(PA)] complexes.

Complex	2θ (deg)	d Value (Å)	β; FWHM	Particle size (nm)
[(Qui)(QL)]	12.694	6.968	0.250	5.827
[(Qui)(PA)]	22.338	3.977	0.225	6.561

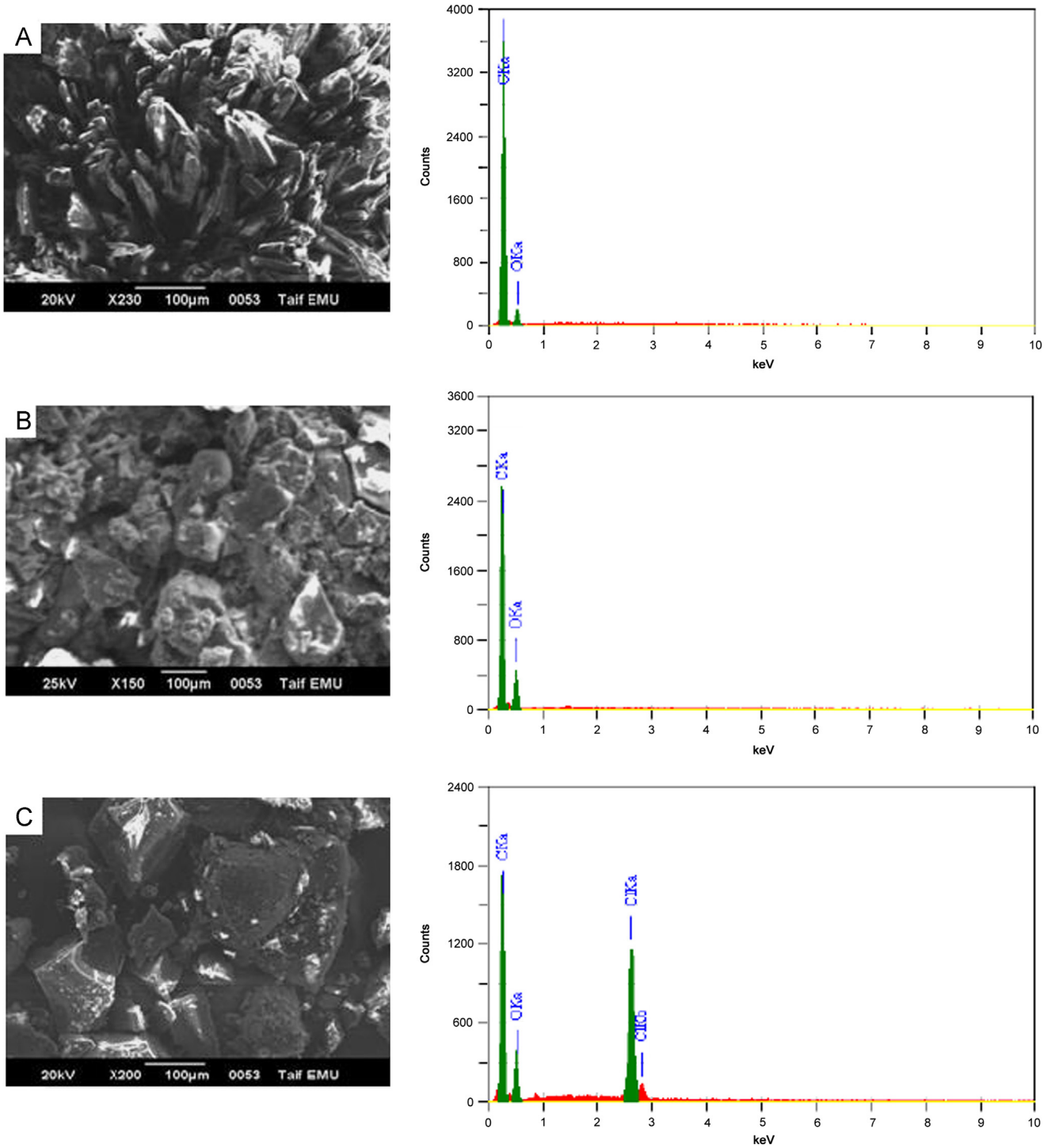

Fig. 10 SEM images and EDX spectrum of (A) [(Qui)(QL)], (B) [(Qui)(PA)] and (C) [(Qui)(DDQ)] complexes.

Table 7 The inhibition diameter zone values (mm) for Qui and its CT complexes.

Sample	Inhibition zone diameter (mm/mg sample)			
	Bacillus subtilis, (G^+)[a]	*Escherichia coli*, (G^-)	*Pseudomonas aeuroginosa*, (G^-)	*Staphylococcus aureus*, (G^+)
Control: DMSO	0.0	0.0	0.0	0.0
Tetracycline (antibacterial agent)	34.0	32.0	34.0	30.0
Qui	7.0	6.0	7.0	5.0
[(Qui)(QL)]	13.0	13.0	12.0	12.0
[(Qui)(PA)]	11.0	12.0	13.0	13.0
[(Qui)(DDQ)]	12.0	12.0	12.0	11.0

[a]G: Gram reaction.

including 2θ, β, d (the interplanar spacing between atoms) and D in nm.

The main characteristic scattering peak of the [(Qui)(QL)] complex occurs at 12.694°, whereas this peak occurs at 22.338° in the diffraction pattern of the [(Qui)(PA)] complex. In the [(Qui)(QL)] complex, appearances of sharp and strong Bragg peak confirm the good crystallinity of this complex. The particle size of the complexes was found to be ~5.8 and ~6.7 nm for the [(Qui)(QL)] and [(Qui)(PA)] complexes, respectively. These values confirmed that the particle sizes are located within the nanoscale range.

3.10. Morphology characterization

The morphology of the Qui CT complexes was determined using scanning electron microscopy (SEM). SEM provides general information about the microstructure, the surface morphology, the particle size, the chemical composition, and the porous structures of the surfaces. In addition, the chemical compositions of the complexes were determined using energy-dispersive X-ray diffraction (EDX). Fig. 10 shows the SEM surface images of the [(Qui)(QL)], [(Qui)(PA)] and [(Qui)(DDQ)] complexes along with their EDX spectra. The formed complexes showed a homogeneous distribution of each acceptor. The sizes of the particles are quite different with different acceptors. Most of the complexes particles exhibit angular shapes with estimated sizes of ~100 μm. The particles of the QL complex are tubular-shaped and those of the PA complex are flake-shaped, whereas the DDQ complex particles appear as agglomerates and display a large surface area. The peaks refer to all elements that constitute the molecules of these complexes; these elements were clearly identified, and the results confirmed the proposed structures.

3.11. Biological activity

The antibacterial activity of the Qui and its complexes were screened *in vitro* against two Gram-positive bacterial strains, *Staphylococcus aureus* (*S. aureus*) and *Bacillus subtilis*, and two Gram-negative bacterial strains, *Escherichia coli* (*E. coli*) and *Pseudomonas aeruginosa* (*P. aeruginosa*). The CT complexes to be tested were dissolved in DMSO to obtain 100 μg/mL stock solutions. The activity was determined by measuring the inhibition zone diameter values (mm) of the complexes against the microorganisms. Tetracycline was used as the positive control. The screening data are listed in Table 7. The results indicated that the Qui complexes exhibited moderate inhibitory results against all of the Gram-positive and Gram-negative bacterial species, as reported in Table 7. It is obvious that the biological activity of the Qui CT complexes is more than that of free Qui drug. In addition, the biological activity of the Qui drug and its complexes are lower than tetracycline standard.

4. Conclusion

Qui is well known as medicinally important compound. This paper described the CT complexes of Qui with three acceptors. The synthesized CT complexes were characterized using various spectroscopic techniques including UV–visible, IR, Raman, ^{1}H NMR spectroscopy and X-ray diffraction as well as scanning electron microscopy and thermogravimetric (TG) analyses. It is observed that the reaction stoichiometry is 1:1, and the resulting CT complexes were shown to have the general formula: [(Qui)(acceptor)]. The obtained complexes are nanoscale, semi-crystalline material, thermally stable and spontaneous. Physical and kinetic parameters such as formation constant (K_{CT}), molar extinction coefficient (ε_{CT}) and other spectroscopic data have been estimated. The CT complexes were also screened for their antibacterial activities using the disc diffusion method, and it is obvious that the antibacterial activity of the Qui CT complexes is more than that of free Qui drug.

References

[1] M.S. Refat, S.A. El-Korashy, I.M. El-Deen, Experimental and spectroscopic studies of charge transfer reaction between sulfa salazine antibiotic drug with different types of acceptors, Drug Test. Anal. 3 (2011) 116–131.
[2] A. Korolkovas, Essentials of Medicinal Chemistry, second ed., Wiley, New York, USA, 1998 (Chapter 3).
[3] I.M. Khan, A. Ahmad, M.F. Ullah, Synthesis, crystal structure, antimicrobial activity and DNA-binding of hydrogen-bonded proton-transfer complex of 2,6-diaminopyridine with picric acid, J. Photochem. Photobiol. B 103 (2011) 42–49.
[4] I.M. Khan, A. Ahmad, M.F. Ullah, Synthesis, spectroscopic investigations, antimicrobial and DNA binding studies of a new charge transfer complex of o-phenylenediamine with 3,5-dinitrosalicylic acid, Spectrochim. Acta A 102 (2013) 82–87.
[5] I.M. Khan, A. Ahmad, M. Aatif, Synthesis, single-crystal characterization, antimicrobial activity and remarkable in vitro DNA interaction of hydrogen-bonded proton-transfer complex of 1,10-phenanthroline with 2,4,6-trinitrophenol, J. Photochem. Photobiol. B 105 (2011) 6–13.
[6] I.M. Khan, A. Ahmad, Synthesis, characterization, structural, spectrophotometric and antimicrobial activity of charge transfer complex of

p-phenylenediamine with 3,5-dinitrosalicylic acid, J. Mol. Struct. 975 (2010) 381–388.
[7] I.M. Khan, A. Ahmad, S. Kumar, Synthesis, spectroscopic characterization and structural investigation of a new charge transfer complex of 2,6-diaminopyridine with 3,5-dinitrobenzoic acid: DNA binding and antimicrobial studies, J. Mol. Struct. 1035 (2013) 38–45.
[8] A.M.A. Adam, Structural, thermal, morphological and biological studies of proton-transfer complexes formed from 4-aminoantipyrine with quinol and picric acid, Spectrochim. Acta A 104 (2013) 1–13.
[9] H.H. Eldaroti, S.A. Gadir, M.S. Refat, et al., Preparation, spectroscopic and thermal characterization of new charge-transfer complexes of ethidium bromide with π-acceptors. In vitro biological activity studies, Spectrochim. Acta A 109 (2013) 259–271.
[10] K. Berka, E. Anzenbacherová, T. Hendrychová, et al., Binding of quinidine radically increases the stability and decreases the flexibility of the cytochrome P450 2D6 active site, J. Inorg. Biochem. 110 (2012) 46–50.
[11] S.M. Sarkar, Y. Taira, A. Nakano, et al., Organocatalytic asymmetric synthesis of quinine and quinidine, Tetrahedron Lett. 52 (2011) 923–927.
[12] T.S. Kaufman, E.A. Rúveda, The quest for quinine: those who won the battles and those who won the war, Angew. Chem. Int. Ed. 44 (2005) 854–885.
[13] J. Seayad, B. List, Asymmetric organocatalysis, Org. Biomol. Chem. 3 (2005) 719–724.
[14] C.E. Song (Ed.), Cinchona Alkaloids in Synthesis and Catalysis: Ligands Immobilization and Organocatalysis, Wiley-VCH, Weinheim, 2009.
[15] T. Marcelli, H. Hiemstra, Cinchona alkaloids in asymmetric organocatalysis, Synthesis 8 (2010) 1229–1279.
[16] D.J. Naas, in: Quinidine, Encyclopedia of Toxicology, second edition, Elsevier B.V. publishing company, 2005, pp. 593–594, http://dx.doi.org/10.1016/B0-12-369400-0/00824-3.
[17] F.H. Fenton, E.M. Cherry, B.G. Kornreich, Termination of equine atrial fibrillation by quinidine: an optical mapping study, J. Vet. Cardiol. 10 (2008) 87–103.
[18] D.J. Beecher, A.C. Wong, Identification and analysis of the antigens detected by two commercial *Bacillus cereus* diarrheal enterotoxin immunoassay kits, Appl. Environ. Microbiol. 60 (1994) 4614–4616.
[19] National Committee for Clinical Laboratory Standards. Methods for Antimicrobial Susceptibility Testing of Anaerobic Bacteria: Approved Standard M11-A3. NCCLS, Wayne, PA, USA, 1993.
[20] A.S.M. Hossan, H.M. Abou-Melha, M.S. Refat, In situ synthesis, photometric and spectroscopic studies of chelating system during the 1,4,7,10,13,16-hexaoxacyclooctadecane charge transfer reaction with different acceptors, Spectrochim. Acta A 79 (2011) 583–593.
[21] R. Rathore, S.V. Lindeman, J.K. Kochi, Charge-transfer probes for molecular recognition *via* steric hindrance in donor–acceptor pairs, J. Am. Chem. Soc. 119 (1997) 9393–9404.
[22] K.M. Al-Ahmary, M.M. Habeeb, E.A. Al-Solmy, Spectroscopic studies of the hydrogen bonded charge transfer complex of 2-aminopyridine with π-acceptor chloranilic acid in different polar solvents, J. Mol. Liq. 162 (2011) 129–134.
[23] A.S. AL-Attas, M.M. Habeeb, D.S. AL-Raimi, Synthesis and spectroscopic studies of charge transfer complexes between chloranilic acid and some heterocyclic amines in ethanol, J. Mol. Struct. 928 (2009) 158–170.
[24] M.S. Refat, L.A. El-Zayat, O.Z. Yesilel, Spectroscopic characterization of charge-transfer complexes of morpholine with chloranilic and picric acids in organic media: crystal structure of bis(morpholinium 2,4,6-trinitrocyclohexanolate), Spectrochim. Acta A 75 (2010) 745–752.
[25] M.S. Refat, H.A. Saad, A.A. Adam, Proton transfer complexes based on some π-acceptors having acidic protons with 3-amino-6-[2-(2-thienyl)vinyl]-1,2,4-triazin-5(4H)-one donor: synthesis and spectroscopic characterizations, J. Mol. Struct. 995 (2011) 116–124.
[26] R. Bharathikannan, A. Chandramohan, M.A. Kandhaswamy, et al., Synthesis, crystal growth and properties of the charge transfer complex adduct of 2-nitro aniline with picric acid – an organic non-linear optical material, Cryst. Res. Technol. 43 (6) (2008) 683–688.
[27] A.S. Gaballa, S.M. Teleb, E. Nour, Preparation and spectroscopic studies on charge-transfer complexes of famciclovir drug with different electron acceptors, J. Mol. Struct. 1024 (2012) 32–39.
[28] A.A. Adam, M.S. Refat, T. Sharshar, et al., Synthesis and characterization of highly conductive charge-transfer complexes using positron annihilation spectroscopy, Spectrochim. Acta A 95 (2012) 458–477.
[29] A.A. Adam, Synthesis, spectroscopic, thermal and antimicrobial investigations of charge-transfer complexes formed from the drug procaine hydrochloride with quinol, picric acid and TCNQ, J. Mol. Struct. 1030 (2012) 26–39.
[30] M.S. Refat, Synthesis, spectroscopic, thermal and antimicrobial investigations of charge-transfer complexes formed from the drug procaine hydrochloride with quinol, picric acid and TCNQ, J. Mol. Struct. 985 (2011) 380–390.
[31] G.G. Mohamed, S.M. Khalil, M.A. Zayed, et al., 2,6-Dichloroquinone chlorimide and 7,7,8,8-tetracyanoquinodimethane reagents for the spectrophotometric determination of salbutamol in pure and dosage forms, J. Pharm. Biomed. Anal. 28 (2002) 1127–1133.
[32] A.S. Amin, M.E. Moustafa, Y.M. Issa, Spectrophotometric microdetermination of ampicillin and amoxicillin with picric and picramic acids, Microchem. J. 50 (1994) 6–13.
[33] N. Singh, A. Ahmad, Spectrophotometric and spectroscopic studies of charge transfer complex of 1-Naphthylamine as an electron donor with picric acid as an electron acceptor in different polar solvents, J. Mol. Struct. 977 (2010) 197–202.
[34] S.J.S. Qazi, A.R. Rennie, J.K. Cockcroft, et al., Use of wide-angle X-ray diffraction to measure shape and size of dispersed colloidal particles, J. Colloid Interface Sci. 338 (2009) 105–110.